

# Organoaqueous calcium chloride electrolytes for capacitive charge storage in carbon nanotube electrodes at sub-zero-temperatures

## Electronic Supplementary Information

Yun Gao,<sup>a,b</sup> Zhanbin Qin,<sup>b</sup> Li Guan,<sup>a</sup> Xiaomian Wang,<sup>b</sup> and George Z. Chen<sup>\*,a,c</sup>

<sup>a</sup> Department of Chemical and Environmental Engineering, and Energy and Sustainability Research Division, Faculty of Engineering, The University of Nottingham, Nottingham NG7 2RD, UK

E-mail: [george.chen@nottingham.ac.uk](mailto:george.chen@nottingham.ac.uk)

<sup>b</sup> Department of Chemical Engineering, North China University of Science and Technology, Tangshan, Hebei 063009, P. R. China

<sup>c</sup> Department of Chemical and Environmental Engineering, and Centre for Sustainable Energy Technologies, Faculty of Science and Engineering, The University of Nottingham Ningbo China, Ningbo 315100, P. R. China

### S1. Experimental

Cyclic voltammetry was carried out on the PGSTAT30 Autolab Potentiostat (Eco Chemie, Inc) with errors typically smaller than 1 mV in potential control and measurement. A one compartment three electrode cell was used for recording cyclic voltammograms. The cell consisted of a 100 mL beaker for containing the electrolyte, a CNT working electrode, a graphite rod counter electrode and an Ag/AgCl (3 mol L<sup>-1</sup> KCl) reference electrode. Specific capacitance of the CNT working electrode was derived from rectangular CVs by  $C_{sp} = \text{total change enclosed in CV curve} / (2 \times \text{potential range} \times \text{CNT mass})$ . The CNT electrodes were prepared by casting and drying (in air) the acid treated CNT suspension with added PTFE (5 wt% after drying) on a graphite disc electrode of 5 mm in diameter (which functioned as the current collector). The measured  $C_{sp}$  values varied in a range up to 30%, depending on several factors, including acid treatment conditions, CNT content in the suspension, total CNT loading on, and surface condition of the disc electrode. For comparison purposes, the as-received powder of a high surface area activated carbon (AC) from Haycarb (<http://www.haycarb.com/>, BET surface area: > 1700 m<sup>2</sup> g<sup>-1</sup>) was mixed with PTFE (8 wt% after drying), dispersed in water in a sonication bath, and then cast on the graphite disc electrode. Drying was carried out in a vacuum oven at 60 °C for >2 h. The slight differences between preparations of the CNT and AC electrodes were because it was more difficult to cast an adherent and uniform AC coating on the graphite disc.

Temperature control and measurement of the electrolyte was achieved using either a dry-ice filled container with a thermocouple for temperature reading in cyclic voltammetry, or an ultralow temperature thermostat bath (DC-8006, CNSHP, Shanghai) working in the temperature range of -80 ~ 100 ± 0.05 °C. All chemicals were used as received from Sigma-Aldrich.

Multi-walled carbon nanotubes (10 ~ 30 nm in diameter) were purchased from CNano (<http://www.cnanotechnology.com/en/>) or Shenzhen Nanotech Port (<http://nami.battery.com.cn/>), and were partially oxidised under refluxation in mixed H<sub>2</sub>SO<sub>4</sub>-HNO<sub>3</sub> (3:1 v:v) for 10~15 min. The acid treated CNTs were washed to neutral pH, dried and stored in sealed glass bottle. The dried CNTs could re-disperse in water (2 g L<sup>-1</sup> in this work) under sonication for casting.

### S2. Cooling curves and phase diagrams

The liquid samples, e.g. mixed formamide and water of ca. 80 mL, were cooled in the ultralow temperature thermostat bath containing anhydrous ethanol (m.p. = -117.3 °C) as the cooling fluid. The bath's working temperature was maintained at -78 °C when recording the cooling curves. Once placed in the bath, the liquid sample temperature was followed and plotted against the time to produce the cooling curves from which data points of thermodynamic interests were collected and analysed. Fig. S1a shows the cooling curves of the formamide-water mixtures at different volume ratios as indicated.

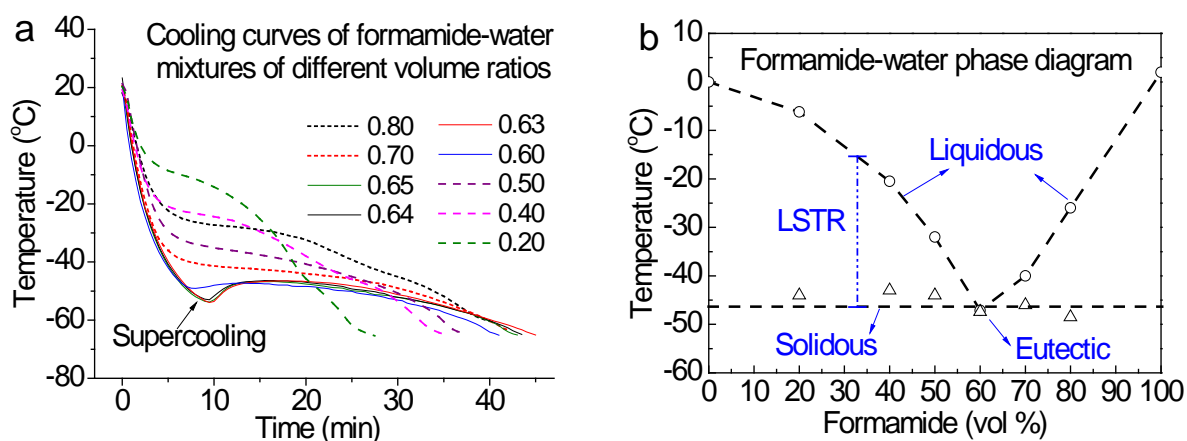


**Fig. S1.** Thermal properties of mixed formamide and water. (a) Cooling curves of formamide-water mixtures at indicated volume ratio measured in a thermostat bath at  $-78\text{ }^{\circ}\text{C}$ . (b) The formamide-water phase diagram. Note in (a) the indicated supercooling phenomenon when the volume ratio of formamide and water approached the eutectic composition. The dashed lines in (b) are presented as a vision guide.

Fig. S2 illustrates the way used in this work to measure the flexion or turning points by tangent extrapolation on the cooling curve. Such obtained values of the liquidus and solidus were used to construct the binary phase diagrams as shown in Fig. S1b. It must be mentioned that, as shown in both Fig. S1a and S2a, solution supercooling was often encountered, which in some cases made it difficult or impossible to determine the solidus temperature from the respective cooling curves. Fig. S2a shows a complicated example of  $2\text{ mol L}^{-1}$   $\text{CaCl}_2$  in water (*ca.* 18 wt%). The cooling curve shows a turning point at about  $-15\text{ }^{\circ}\text{C}$  which agrees broadly with the liquidus temperature on the  $\text{CaCl}_2\text{-H}_2\text{O}$  binary phase diagram as shown in Fig. S3.<sup>S1a, S1b</sup> Another change on the cooling curve was expected at the eutectic temperature (*ca.*  $-52\text{ }^{\circ}\text{C}$ ). However, this was not shown clearly on the cooling curve. Instead, below the liquidus point ( $-15\text{ }^{\circ}\text{C}$ ), the temperature decreased to a lowest point of  $-70.9\text{ }^{\circ}\text{C}$  and then increased to a peak at  $-66.2\text{ }^{\circ}\text{C}$ . This behaviour is indication of supercooling, but it was unexpected because crystals must have appeared at and after the liquidus point and helped prevent the remaining solution from supercooling. A possible explanation is that  $\text{CaCl}_2$  is capable of formation of several crystal structures of mono-, di-, tetra-, and hexa-hydrate. Formation of crystals of  $\text{CaCl}_2\cdot 6\text{H}_2\text{O}$  is expected in a properly controlled cooling process according to the  $\text{CaCl}_2\text{-H}_2\text{O}$  phase diagram. However, the cooling experiment in this work was by no means ideal, and thus might have enabled formation of crystals of the lower hydrates via either decomposition of  $\text{CaCl}_2\cdot 6\text{H}_2\text{O}$ , or reaction between  $\text{CaCl}_2$  and  $\text{H}_2\text{O}$ , leading to the complicated cooling behaviour, including supercooling as shown in Fig. S2a.

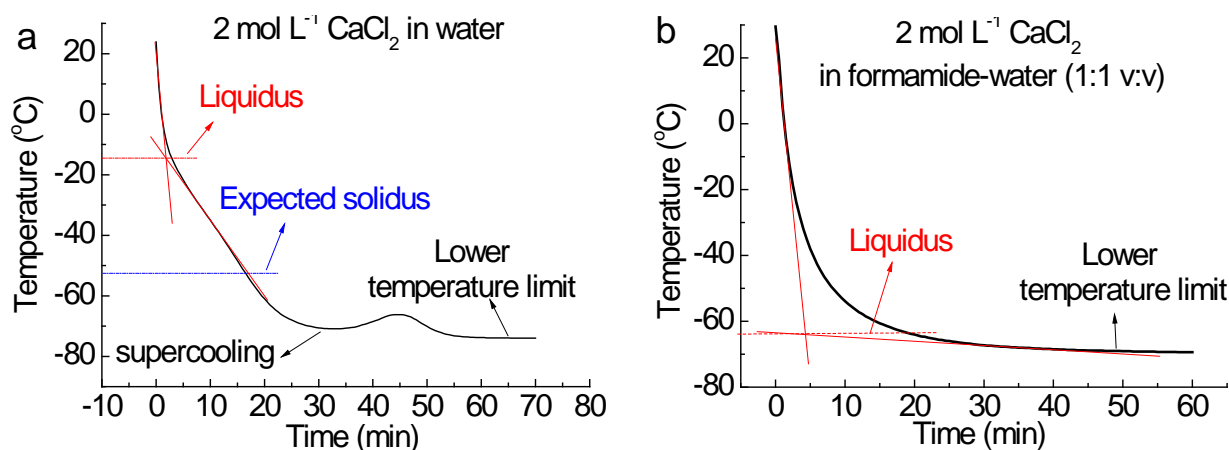


**Fig. S2.** Cooling curves of  $2.0\text{ mol L}^{-1}$   $\text{CaCl}_2$  solutions (a) in water, and (b) in mixed FA- $\text{H}_2\text{O}$  (1:1, v:v).

It is also worth stating that the ultralow temperature thermostat bath could only work to a lowest temperature of  $-78\text{ }^{\circ}\text{C}$  which is very close to the supplier specified lower temperature limit. Consequently, no thermal properties were measurable below  $-78\text{ }^{\circ}\text{C}$ . In fact, even at  $-70\text{ }^{\circ}\text{C}$ , the measured temperature decrease in the sample solution became very slow. As shown in both Fig. S2a and S2b, the plateau near the end of the cooling curve is more likely an indication of the sample temperature approaching the lower limit of the bath, instead of any meaningful thermal behaviour. On the other hand, the cooling curves in Fig. S2b can be taken as a strong indication that the organoaqueous solution of  $2\text{ mol L}^{-1}$   $\text{CaCl}_2$  in the FA- $\text{H}_2\text{O}$  mixture (1:1, v:v) should have a solidus temperature below  $-80\text{ }^{\circ}\text{C}$ . Combining with the CVs in Fig. 2a of this paper, the findings from this work suggest strongly that the  $\text{CaCl}_2$ -FA- $\text{H}_2\text{O}$  solutions are very useful electrolytes for electrochemical applications at sub-zero temperatures.

Note: Fig. S3b shows a eutectic point of  $-60\text{ }^{\circ}\text{C}$  for  $\text{KAc-H}_2\text{O}$  which however has a lower ion conductivity and is more expensive to prepare compared with  $\text{CaCl}_2\text{-H}_2\text{O}$ .

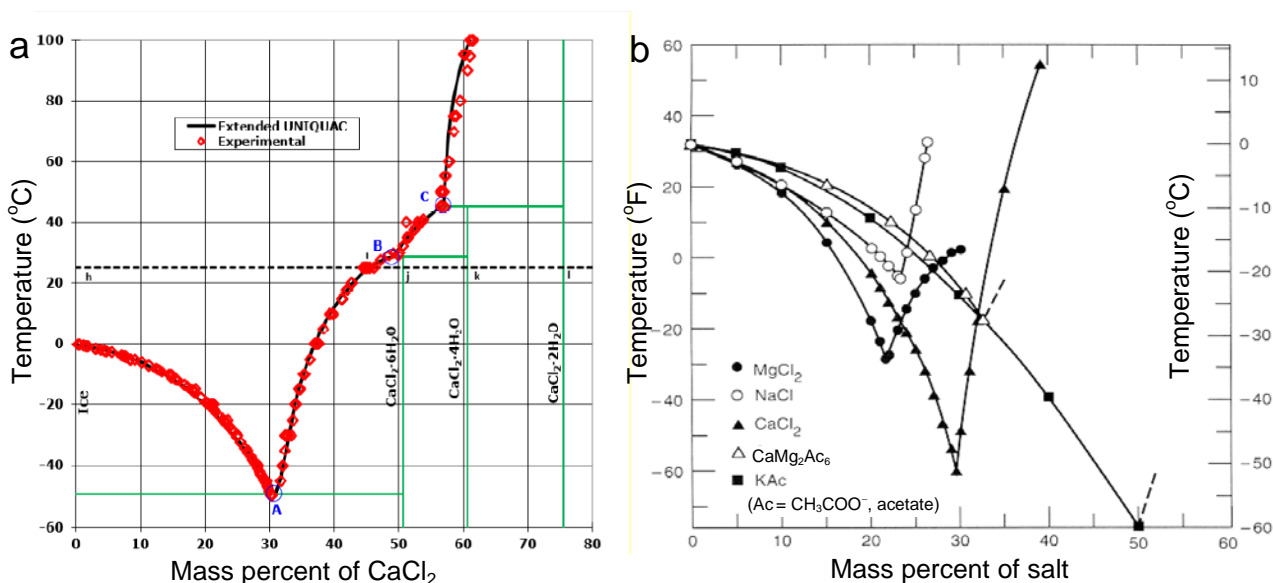


**Fig. S3.** Phase diagrams of  $\text{H}_2\text{O}$  and (a)  $\text{CaCl}_2$  and (b)  $\text{CaCl}_2$ ,  $\text{MgCl}_2$ ,  $\text{NaCl}$ ,  $\text{CaMg}_2\text{Ac}_6$  (CMA), or  $\text{KAc}$ .<sup>S1a, S1b</sup>

### S3. Comparison between cyclic voltammograms of CNTs and AC in $\text{CaCl}_2$ and $\text{KCl}$ electrolytes

For comparison, CVs of the CNT electrode were recorded in both the  $\text{CaCl}_2$  and  $\text{KCl}$  electrolytes under the same experimental conditions. It was found in all cases that the capacitance of the acid treated CNT electrode as derived from the CVs was always higher in the  $\text{CaCl}_2$  solution than in the  $\text{KCl}$  solution. Fig. S4 compares the CVs recorded after 5 potential cycles in 1.0 and 0.5  $\text{mol L}^{-1}$  solutions of  $\text{KCl}$  and  $\text{CaCl}_2$  at room temperature. It can be seen clearly that the CVs recorded in the  $\text{CaCl}_2$  solutions exhibit greater currents than that in the  $\text{KCl}$  solutions, **corresponding to about 30% increase in capacitance**. This observation agrees with the expected stronger affinity between the  $\text{Ca}^{2+}$  ion and the oxy-groups, *e.g.* carboxyl, on the CNT surface. Also, it can be seen that the CV currents are greater at more negative potentials in solutions of both  $\text{KCl}$  and  $\text{CaCl}_2$ . This phenomenon may also be attributed to the oxy-groups on the CNT surface being more affinitive to cations ( $\text{K}^+$  or  $\text{Ca}^{2+}$ ) than anions ( $\text{Cl}^-$ ). Interestingly, the concentration change (1.0 and 0.5  $\text{mol L}^{-1}$  in Fig. S4a and S4b, respectively) had a fairly small influence on the CV current and shape, which is indicative of the charge (or ion) storage in the electrode being determined mainly by the available sites on the CNT surface for ion sorption, instead of the number of ions in the electrolyte.

Further investigation is still ongoing in our laboratory on the influences of alkali and alkaline earth cations on the electrochemical properties of CNTs and various other carbons, *e.g.* activated carbon and graphene. As a preliminary test, CVs of the Haycarb AC were recorded in both the aqueous  $\text{KCl}$  and  $\text{CaCl}_2$  electrolytes with some typical results presented in Fig. S4c and S4d. It can be seen that the Haycarb AC

worked very well in both the KCl and CaCl<sub>2</sub> electrolytes for capacitive charge storage, and offered slightly higher capacitance in CaCl<sub>2</sub>. However, the capacitance gain is noticeably smaller for AC than for CNT, which may be explained as follow.

The Haycarb AC has a high specific surface area of over 1700 m<sup>2</sup> g<sup>-1</sup>, and hence should exhibit specific capacitance of 170~340 F g<sup>-1</sup> assuming only contribution from the electric double layer which is known to have area normalised capacitance between 10~20 μF cm<sup>-2</sup>. The specific capacitance derived from CVs recorded at low potential scan rates as shown in Fig. S4d ranged between 120 and 130 F g<sup>-1</sup> which are much smaller than the prediction given above. This finding suggests that firstly not all the pores in the AC are accessible by the ions, and secondly there could be very little, if not zero, contribution from the oxy-groups, if any, in the AC electrode. The second reason can account for the relatively small difference between the CVs of the Haycarb AC in KCl and CaCl<sub>2</sub> in comparison with the CVs of CNTs. A possible scenario is that the number of oxy-groups per unit surface in the Haycarb AC is significantly smaller than that in the acid treated CNTs. Alternatively, one may consider that the oxy-groups in the AC may be mostly hidden in small pores, and hence not accessible by ions from the electrolyte.

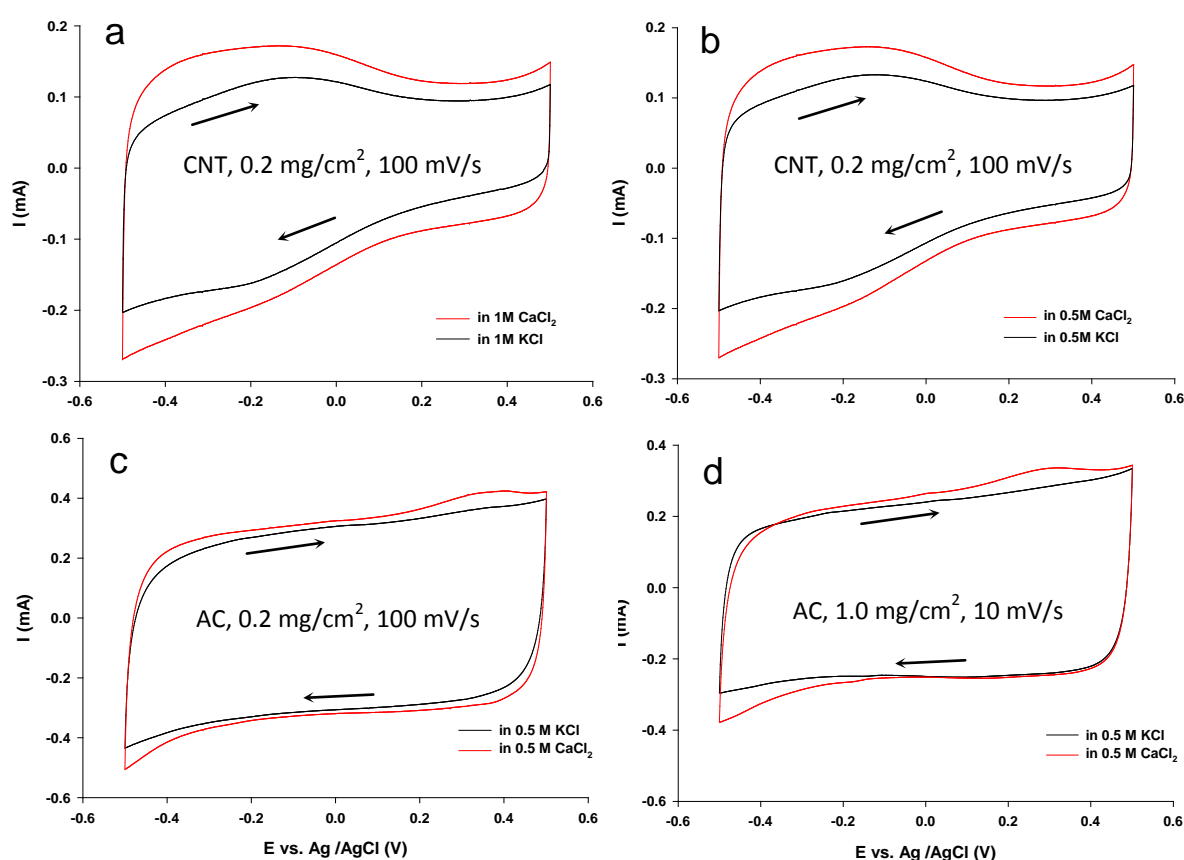


**Fig. S4.** Cyclic voltammograms of acid treated CNTs (a, b) and activated carbon (c, d) coated graphite electrode in 1.0 (a) and 0.5 mol L<sup>-1</sup> (b, c, d) solutions of CaCl<sub>2</sub> (red lines) and KCl (black lines) at 100 mV s<sup>-1</sup> (a, b, c) and 10 mV s<sup>-1</sup> (d) and room temperature. Arrows indicate the direction of the potential scan.

#### S4. Morphology of the CNT coating on the graphite disc electrode

Fig. S5 show the SEM images of the surface of the CNT electrode before and after potential cycling in the CaCl<sub>2</sub>-FA-H<sub>2</sub>O electrolyte at - 60 °C. These two images were taken directly from the CNT electrode without using any conductive coating. In Fig. S5a, the randomly packed and entangled nanofibrils are clearly visible as expected from casting the CNT suspension and drying. After repeated potential cycling at - 60 °C, the

CNT electrode was removed from the electrolyte, dried in air and inspected directly in the SEM chamber. By doing so, it was hoped to avoid alteration of the surface morphology that may be caused by washing or coating. However, the electrode must have contained the  $\text{CaCl}_2$  salt which cannot be removed by vacuum drying. The presence of  $\text{CaCl}_2$  is evidenced by some white spots appearing in Fig. S5b, obviously resulting from electric charging on the insulating crystallites of anhydrous or hydrated  $\text{CaCl}_2$ . In addition, the CNTs in Fig. S5a are fairly closely packed whilst the gaps between individual CNTs are still clearly seen. However, in Fig. S5b, the CNTs are wider separated, and there appear in the image some blurred regions around and between the CNTs that seem to be amorphous phases. The wider separation between CNTs indicates expansion of the CNT coating, and could have resulted from repeated ingress and egress of the ions in the CNT coating during potential cycling. The amorphous phases present around and between the CNTs could be the dried but uncrystallised  $\text{CaCl}_2$  in association with  $\text{H}_2\text{O}$  and/or FA molecules that could not be removed by the vacuum in the SEM chamber. The fact that these amorphous phases did not produce the charging effect in the SEM image suggests some levels of conductivity which could be ionic in nature assisted by the presence of solvent molecules. It should be mentioned that our explanation of Fig. S4b is still speculative and further studies are needed for confirmation.

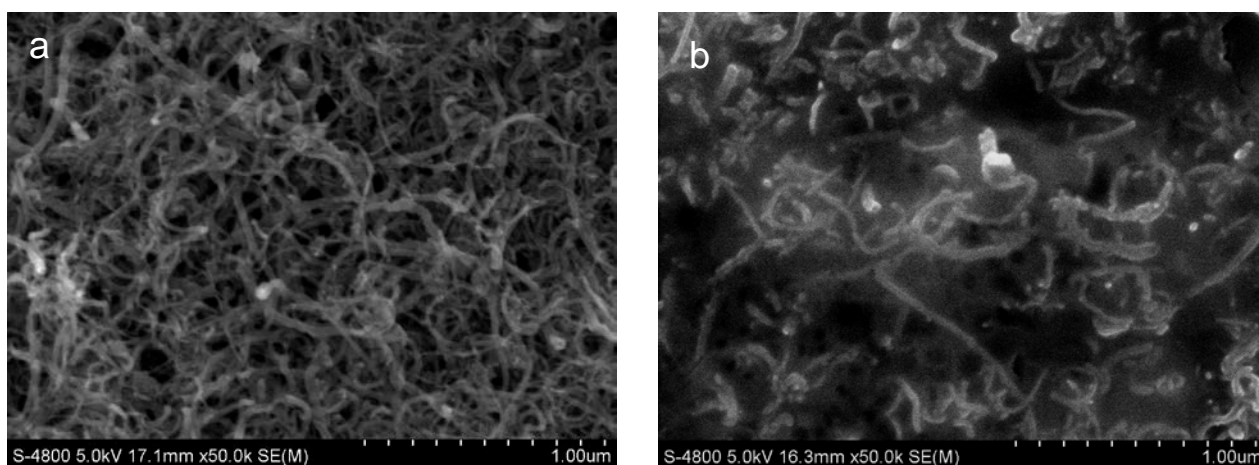


**Fig. S5.** SEM images showing the surface morphologies of the CNT electrode before (a) and after (b) repeated potential cycling in the  $\text{CaCl}_2$  ( $2.0 \text{ mol L}^{-1}$ )-FA- $\text{H}_2\text{O}$  solution at  $-60^\circ\text{C}$ .

### S5. Further discussion on the affinity between calcium cations and oxy-groups on CNT surfaces

To further elaborate the unique affinity between the  $\text{Ca}^{2+}$  ion and the oxy-groups on the CNT surface, it is worth mentioning some early and relevant studies reported in the literature. The first example is the so called Calcium Ionophore A23187 or Antibiotic A23187.<sup>S1c, S1d</sup> It is an antibiotic and ionophore, and has high selectivity for binding and transporting the  $\text{Ca}^{2+}$  ion over other cations, such as  $\text{Na}^+$ ,  $\text{K}^+$  and  $\text{Mg}^{2+}$  ions in biological systems. According to supramolecular chemistry, this high  $\text{Ca}^{2+}$  ion selectivity of A23187 can be explained by the various oxygen containing groups in the ionophore molecule forming a  $\text{Ca}^{2+}$  ion binding site/cavity as illustrated in Fig. S6a. In addition to the compatibility between the binding cavity and the  $\text{Ca}^{2+}$  ion in terms of size and shape, the high affinity between oxygen and calcium must have also made a great contribution towards the observed  $\text{Ca}^{2+}$  selectivity of A23187.

In similar terms, we assume the oxy-groups on CNT surfaces can also offer high selectivity for  $\text{Ca}^{2+}$  ions as schematically illustrated in Fig. S6b. This assumption is in agreement with many previous studies involving interactions between CNTs and  $\text{Ca}^{2+}$  ions. It was reported that according to molecular dynamic simulation, the interaction between the carboxylate group on CNTs and  $\text{Ca}^{2+}$  ions are more favourable over  $\text{K}^+$  and  $\text{Na}^+$  ions.<sup>S2a</sup> In an experimental study, as-prepared CNTs (which must contain surface oxy-groups)

were demonstrated to be effective scaffold materials for osteoblast proliferation and bone formation, thanks to partly the ability of the CNTs to conduct  $\text{Ca}^{2+}$  currents.<sup>S2b</sup> It was also experimentally observed that in comparison with  $\text{Na}^+$ ,  $\text{K}^+$ , and  $\text{Mg}^{2+}$  ions, the  $\text{Ca}^{2+}$  ion was the more effective cation to coagulate and precipitate suspended CNTs in water.<sup>S2c, 2d</sup>

Last, but not the least, oxy-groups are known to be present in many carbon materials, but their interactions with the  $\text{Ca}^{2+}$  are not expected to be the same. This is because for CNTs, and also possibly graphenes, the oxy-groups are present on the surfaces or edges and hence can interact well with the  $\text{Ca}^{2+}$  ions. However, there are many types of AC materials with vastly different structures and oxy-functionalities. For those ACs with well exposed and arranged oxy-groups, good interactions with the  $\text{Ca}^{2+}$  ion can be anticipated. If the oxy-groups are hidden inside the structure, or do not form an appropriate structures like those shown in Fig. S6, there may not be a significant benefit from using the  $\text{Ca}^{2+}$  ion in the electrolyte for capacitance gain. Nevertheless, the effect of  $\text{CaCl}_2$  to lowering the liquidus temperature of the organoaqueous electrolyte is still a plus point for applications at sub-zero temperatures.

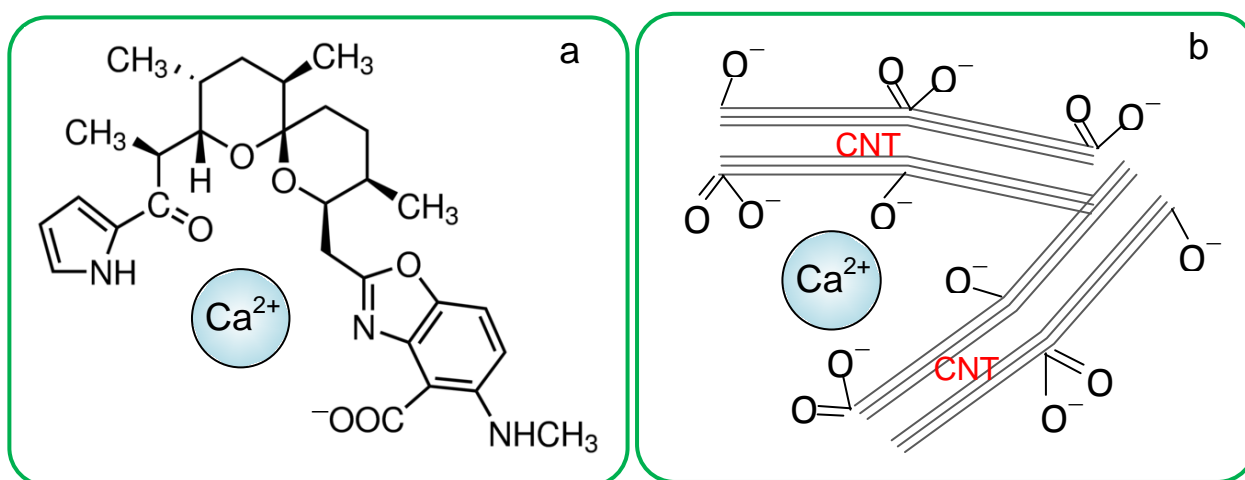


**Fig. S6.** Schematic illustration of the binding of a  $\text{Ca}^{2+}$  ion by the oxy-groups in the cavity formed (a) in the Calcium Ionophore A23187 molecule, and (b) in between the CNTs.

#### Supplementary References

- S1. (a) [http://www.phasediagram.dk/binary/calcium\\_chloride.htm](http://www.phasediagram.dk/binary/calcium_chloride.htm);  
 (b) <http://www.fhwa.dot.gov/publications/research/safety/95202/005.cfm>;  
 (c) <http://en.wikipedia.org/wiki/A23187>;  
 (d) <http://www.sigmaaldrich.com/catalog/product/sigma/c7522?lang=zh&region=CN>.
- S2. (a) R. Garcia-Fandino, M. S. P. Sansom, *PNAS*, 2012, 109, 6939–6944; (b) L. P. Zanello, B. Zhao, H. Hu, R. C. Haddon, *Nano Lett.*, 2006, 6, 562–567; (c) K. Yang, Z.-L. Yi, Q.-F. Jing, D.-H. Lin, *Zhejiang Univ-Sci A*, 2014, 15, 624-633; (d) H. Wang, H. Nie, Y. Wang, Y. Chang, E. Dong, S. Yang, *China Patent*, CN101885527-A, Nov. 2010.